ACS APPLIED NANO MATERIALS

www.acsanm.org Article

Twisted Bilayer Graphene: A Versatile Fabrication Method and the Detection of Variable Nanometric Strain Caused by Twist-Angle Disorder

Andreij C. Gadelha, Douglas A. A. Ohlberg, Fabiano C. Santana, Gomes S. N. Eliel, Jessica S. Lemos, Vinícius Ornelas, Daniel Miranda, Rafael Battistella Nadas, Kenji Watanabe, Takashi Taniguchi, Cassiano Rabelo, Pedro Paulo de Mello Venezuela, Gilberto Medeiros-Ribeiro, Ado Jorio, Luiz Gustavo Cançado, and Leonardo C. Campos*

Cite This: *ACS Appl. Nano Mater.* 2021, 4, 1858−1866 Read Online

ACCESS | Metrics & More | Article Recommendations | Supporting Information

ABSTRACT: Twisted bilayer heterostructures (TBHs) are materials whose physical properties depend on the twist angle between the two layers of two-dimensional (2D) materials. Those heterostructures are not found in nature, and it is quite common to fabricate them with a nonhomogeneous twist angle, giving rise to the so-called twist-angle disorder. The most reliable method used to fabricate TBHs is the tear-and-stack method, which enables production of TBHs starting from a crystal of hexagonal boron nitride that works as a stamp. However, the twisted 2D materials stay attached to the boron nitride permanently. In this paper, we present a pyramid trunk stamp that enables a versatile and easy fabrication of twisted heterostructures without the aid of boron nitride crystals. The semipyramidal stamp enables good visualization of the 2D materials, easy alignments, and transfer of 2D materials between different substrates, and the same stamp can be reused for many fabrications. We demonstrate our method producing twisted bilayer graphene (TBG), and we present an investigation based on nano-Raman hyperspectral imaging, which can be implemented to characterize regions of TBG under twist-angle disorder, strain, or doping.

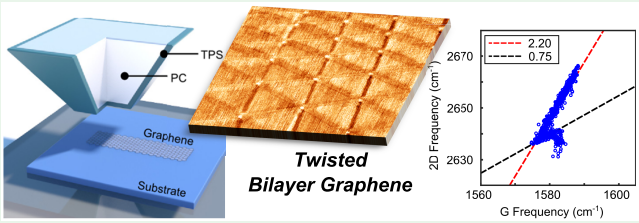

KEYWORDS: *twisted bilayer graphene, tear-and-stack method, strain, scanning microwave impedance microscopy, scanning tunneling microscopy, nano-Raman*

■ INTRODUCTION

Van der Waals heterostructures are unique platforms for studying strongly correlated physics. One exotic example is the twisted bilayer graphene (TBG) with a twist angle close to the so-called "magic angle" ($\theta \sim 1.1°$). This special two-dimensional (2D) material shows phase transitions from a conducting system to a correlated insulator phase, a ferromagnetic phase, and superconductivity.[1−10] These quantum properties arise from the formation of a flat band responsible for strongly interacting effects.[11−15] Not only TBG but other 2D systems like twisted double-bilayer graphene[16] and twisted bilayer transition-metal dichalcogenides also show strongly correlated phases.[17,18] In essence, the central knob that tunes the interaction strength and raises such quantum properties in twisted bilayer heterostructures (TBHs) is the ability to stack twisted 2D materials with meticulous precision.

So far, most reliable ways of transferring 2D materials between any substrates use a polymeric platform.[19−21] However, to manipulate 2D materials and produce TBH, it is crucial to have technologies and procedures that enable layer-by-layer pick-up, rotation, and precise subsequent stacking of 2D materials.[22,23] The pick-up method is a significant improvement in sample preparation for twistronics. It takes advantage of the bidimensional nature of the 2D materials to stack them together and form a molecular "Lego", whose properties are tuned by the choice of one out of a countless continuum of rotational angles. Nevertheless, to achieve angular control and produce TBHs, the best approach so far is to take advantage of the pick-up technique and use it to tear-and-stack different regions of the same 2D layer.[22,24] More recently, it has been shown that by using a microdome polymer stamp, it is possible to perform three-dimensional (3D) manipulations of 2D materials, like folding, rotating, sliding, and exfoliating.[26] Although these techniques paved the

Received: December 5, 2020
Accepted: February 2, 2021
Published: February 15, 2021

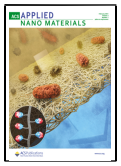

Downloaded via Leonardo Campos on April 20, 2021 at 19:57:22 (UTC).
See https://pubs.acs.org/sharingguidelines for options on how to legitimately share published articles.

ACS Publications © 2021 American Chemical Society

https://dx.doi.org/10.1021/acsanm.0c03230
ACS Appl. Nano Mater. 2021, 4, 1858−1866

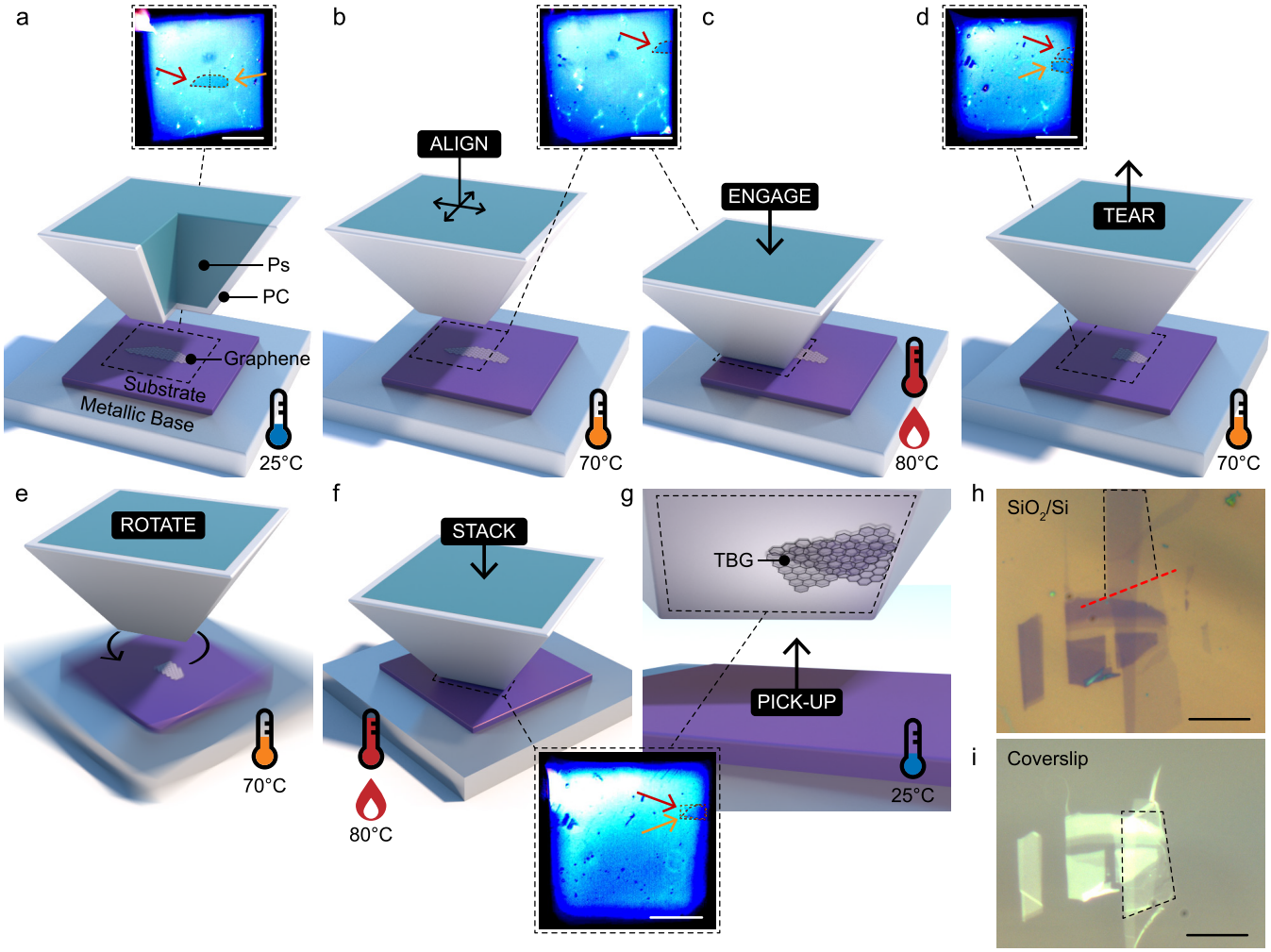

Figure 1. Tear-and-stack to build TBG using the PS. (a) Visualizing the graphene flake though the PS. (b) Beginning of the tear process. The PS is aligned over a region of a graphene sheet. (c) PS in contact with part of the graphene sheet while the temperature is raised. (d) PS cooled down and retracted from the graphene sheet, tearing and picking up the section of sheet previously in contact with the PS. (e) PS aligned over the remaining half of the graphene sheet, which is then rotated by the desired twist angle. (f) PS pressed in contact with the rotated section of the graphene sheet while the temperature is raised. (g) Sample cooled down, separating the PS from the sample. The TBG stays attached to the PC that covers the PS. The scale bar depicted in the optical pictures presented in panels a−g is 50 μm. (h) Optical micrograph of a graphene sample on a SiO_2/Si substrate before the tear-and-stack process. (i) Same transferred to a coverslip after a tear-and-stack procedure. The scale bar depicted in panels h and i is 10 μm.

way for fantastic applications, producing a clean TBH with a high precision angle between the two sheets is still challenging.

The tear-and-stack method renders high-quality TBH samples.[24,25] The most common method uses a combination of a hemispherical poly(dimethylsiloxane) (PDMS) and a hexagonal boron nitride (hBN) stamp to tear a 2D material in two pieces and stack them together with the desired angle.[24] Electronic transport groups widely employ this method;[1,2,27,28] however, it leaves a capping hBN flake on top of the TBH, which hinders near-field[29,30] interactions and scanning probe microscopy investigations.[31] One option involves an additional procedure in the fabrication process to overcome this pertinent issue, by transferring the hBN/TBH system to an intermediate substrate before the final transfer to the target substrate.[32] Nonetheless, this procedure has many steps and can yield a poor-quality TBH. Besides, the conventional tear-and-stack method cannot lead to scalable TBH production because hBN flakes have uncontrolled sizes and availability. One option that does not require any hBN target crystal is a tear-and-stack method based on wetting-induced delamination.[33]

Here, we present a versatile pyramid trunk PDMS stamp that does tear-and-stack without hBN, eases 2D material visualization, and is conducive to several nanomanipulation methods.[29] The so-called pyramid stamp (PS) is fabricated with precisely controlled dimensions by standard clean-room fabrication (see the Supporting Information). The PS is durable, and a single stamp can be used for multiple operations. We validate our method by making TBG samples via a versatile tear-and-stack method and transferring them to different substrates. The quality of the samples is evaluated by atomic force microscopy (AFM), near-field scanning microwave impedance microscopy (sMIM), and scanning tunneling microscopy (STM). We show that micro-Raman and nano-Raman spectroscopy can be implemented as noninvasive techniques able to distinguish strained and doped regions of TBG on hBN crystals. Such an analysis is blurred if the TBG is sitting on SiO_2/Si substrates possibly because of spatial charge

https://dx.doi.org/10.1021/acsanm.0c03230
ACS Appl. Nano Mater. 2021, 4, 1858−1866

inhomogeneity. Finally, we show that nano-Raman spectroscopy is capable of detecting local strain in TBG on hBN crystals, and variable local strain is present in TBG samples because of twist-angle disorder.

■ RESULTS AND DISCUSSION

We begin illustrating how the PS is used to do versatile tear-and-stack of a graphene flake (Figure 1). First, the PS is covered with a polycarbonate (PC) sheet, as we show schematically in Figure 1a (see the Methods section for details). The top panel of Figure 1a shows an optical micrograph of a graphene sheet through the PS. Because of the PS flat surface, the graphene is clearly observed below it. The substrate is initially heated up to a temperature of T = 70 °C, and then the PS edge is aligned to partially cover a graphene flake (Figure 1b). Figure 1b also shows an optical micrograph of the alignment procedure. Next, the PS is contacted with the graphene still at T = 70 °C (Figure 1c). At this temperature, approximation and separation between the graphene and PS can be performed several times until reaching a desired contact. After reaching the desired alignment, we tear the graphene flake. For that, keeping the PS in contact, the temperature is raised from T = 70 to 80 °C (Figure 1c). After 1 min of contact, the sample is cooled to T = 70 °C. Similar to the pick-up method,[22,24] after the temperature is ramped up and down, the graphene flake sticks to the PC. The PS is then retracted, removing the piece of graphene underneath it from the substrate (Figure 1d). Figure 1d presents an optical micrograph of the torn graphene as seen through the PS, indicated by the red arrow. Moreover, the remaining piece of graphene on the substrate can also be observed, as indicated by the orange arrow in Figure 1d. Next, the base is precisely rotated (Figure 1e), and the two parts of graphene are stacked together (Figure 1f). The previous temperature ramp and cooldown process is then repeated to remove the remaining piece. In the end, the two parts of the original graphene flake stay attached to the PC that covers the PS (Figure 1g). Figure 1g also exhibits an optical micrograph of the TBG on top of the PS.

The tear-and-stack method using the PS is advantageous because the TBH can be transferred to any substrate by detaching the PC[22] because there is no hBN flake atop. In order to transfer the TBG, one needs to choose a target substrate, put the PS in contact, and raise the temperature to T = 180 °C. At this temperature, the PS is retracted, transferring the TBG and PC layer to the substrate. Next, the PC layer is removed in chloroform and isopropyl alcohol baths (15 min at 40 °C in chloroform and 1 min in an isopropyl alcohol bath at room temperature). For illustration purposes, Figure 1h presents an optical micrograph of a graphene flake on a SiO_2/Si substrate prior to the tear-and-stack process. Then, graphene is torn at the dashed red line; the graphene region inside the black dashed line is picked up and stacked onto the remaining piece. Afterward, the formed TBG is transferred to a coverslip substrate (Figure 1i). In Figure 1i, we observe the graphene inside the black dashed line stacked on the remaining graphene piece. The contact between the PC and TBG could lead to residue contamination, but we show here by sMIM, Raman spectroscopy, and STM that our TBG samples are clean.

In order to validate the reliability of the tear-and-stack method using the proposed PS, we produced several TBGs sitting on SiO_2 and hBN/SiO_2 substrates with small twist angles. All fabricated TBGs are high-quality samples, and we observe twist-angle-dependent Moiré patterns[34−37] and atomic reconstructions.[38] In Figure 2, we show images of sMIM with

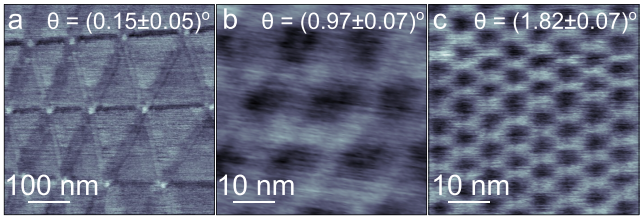

Figure 2. Visualizing Moiré patterns by near-field sMIM. (a) sMIM measurement of a crystal reconstruction observed on a TBG with a small twist angle $\theta \sim 0.15°$. TBG on top of an hBN crystal on SiO_2. (b) sMIM measurement of a Moiré crystal lattice observed on a TBG with a twist angle close to $\theta \sim 0.97°$. (c) sMIM measurement of a Moiré crystal lattice observed with a twist angle of $\theta \sim 1.82°$. TBGs in parts b and c are on top of SiO_2 substrates.

resolution down to 1 nm of three TBG samples. These images are the conductance component of the reflected microwave signal, which is a function of the local conductivity of the sample.[39] The scanning technique is versatile and clearly shows the formation of lattice reconstruction on a TBG sample with a small angle $\theta = 0.15 \pm 0.05°$ (Figure 2a). This sample is on top of an hBN/SiO_2 substrate. The image reveals the triangular-like domains associated with Bernal AB−BA regions.[29,38] Interfaces with different reflectances are observed, at the boundaries between Bernal regions, which we interpret as the soliton regions. Bright spots associated with AA stacking regions can be seen at the vertices of the triangular domains. Figure 2b shows an example of a TBG with twist angle very close to the magic angle $\theta = 0.97 \pm 0.07°$. This TBG is on top of a SiO_2 substrate. Again, the sMIM image reveals bright and dark spots following a Moiré superlattice. Moreover, as expected,[34] the periodicity of the Moiré superlattice decreases with increasing twist angle, as shown in Figure 2c for a TBG with a larger twist angle $\theta = 1.82 \pm 0.07°$. This TBG is also on top of a SiO_2 substrate. All data shown in Figure 2 were taken at room temperature and ambient conditions. Indeed, sMIM is a practical scanning probe technique but is also sensitive to sample contaminants. Using the PS technique, a dozen samples were fabricated, and all of them were clean enough to observe Moiré patterns with a scanning probe technique.

The PS also can be implemented to transfer a TBH between different substrates. To illustrate this capability, in Figure 3, we show a sMIM characterization of a TBG ($\theta \sim 1°$) initially fabricated on a SiO_2 substrate (see optical micrographs and more details in the Supporting Information). The image in Figure 3a corresponds to the in-phase component of the reflected microwave signal, which clearly shows the changes in the local conductivity of a Moiré superlattice with a periodicity of 14.06 ± 0.04 nm, corresponding to twist angle $\theta = 0.96 \pm 0.01°$. After characterization of the sample with sMIM, the TBG was transferred to a mica substrate coated with an atomically flat layer of gold for STM measurement (mica/Au).

The sample, now STM-compatible, was introduced to a UHV VT STM/AFM model scanning tunneling microscope manufactured by Omicron GmbH, where we measured the sample in a vacuum at a base pressure of 1.0×10^{-10} Torr. In Figure 3b, an STM current image was acquired over the TBG, at approximately the same region where the sMIM data were

https://dx.doi.org/10.1021/acsanm.0c03230
ACS Appl. Nano Mater. 2021, 4, 1858−1866

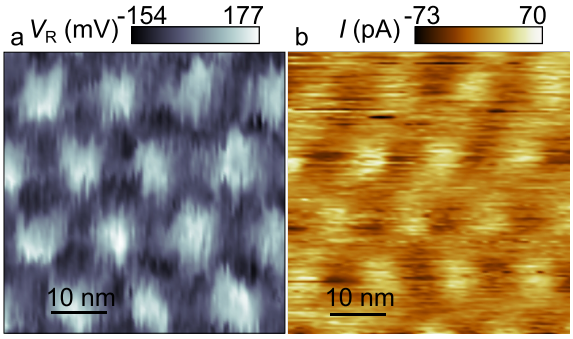

Figure 3. sMIM and STM characterizations of a TBG transferred from SiO_2 to mica/Au substrates. (a) sMIM characterization of the TBG on the SiO_2 substrate. (b) STM image of the TBG on the mica/Au substrate.

collected previously. The image was collected in a constant-current mode with a tip bias of 1 V and a feedback current of 500 pA. The Moiré superlattice measured by STM shows a periodicity of 13.99 ± 0.09 nm, which corresponds to a twist angle θ = 1.00 ± 0.01°. Despite the significant challenge of precisely locating the same regions for a sMIM and STM comparison, the twist angles inferred from the periodicity in Figure 3a,b are remarkably close, indicating areas in close proximity. Notably, the quality of the sMIM and STM data shows that the PS transfer technique provides stable and reasonably clean TBG samples. We also provide, in Figure S5, AFM maps comparing the wrinkles and bubbles observed before and after transfer of the sample presented in Figure 4.

To investigate the structural quality and homogeneity of the TBG produced by the tear-and-stack method, we performed

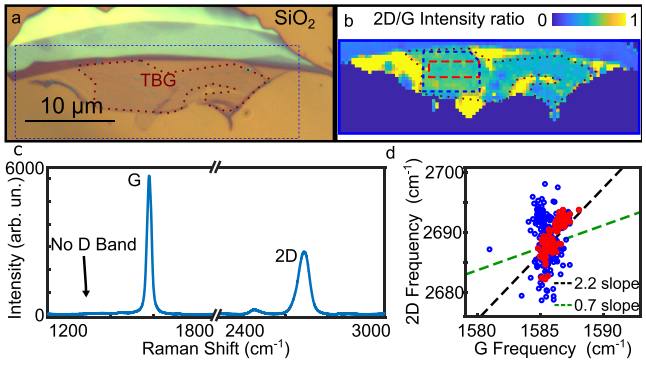

Figure 4. Micro-Raman characterization of the TBG on a SiO_2/Si substrate. (a) Optical image of the TBG on a SiO_2 substrate. (b) Hyperspectral Raman map extracted from the dashed region in part a, in which the color scale renders the 2D/G intensity ratio. Although values of up to 2.5 can be observed over the single-layer graphene areas surrounding the TBG, the color scale was saturated at 1 to highlight the TBG region. The green shades (delineated by dotted lines) span over the TBG area, the yellow shades cover single-layer graphene areas, and the blue shades indicate multilayer graphene. A laser power lower than 2 μW was used to avoid sample heating. (c) Representative micro-Raman spectrum of the same TBG shown in part a, with the sample sitting on the SiO_2 substrate. (d) Plot of ω_{2D} versus ω_G for the TBG data extracted from the hyperspectral Raman matrix that gave rise to the image shown in part b. Blue and red bullets are data points extracted from the areas delimited by the blue and red dashed lines in part b, respectively. Lines with slopes of 2.2 (dashed black line) and 0.75 (dashed green line) are plotted for reference.

Raman spectroscopy measurements. In Figure 4a, we show an optical picture of a TBG sample sitting on the SiO_2 substrate. This is the same TBG characterized by sMIM and STM that is shown in Figure 3. In Figure 4b, we also present a hyperspectral Raman map extracted from the rectangular dashed region in Figure 4a, where the color scale represents the ratio between the intensities of the 2D and G Raman spectra. Although the values go up to 2.5 in the monolayer regions, the color scale was saturated at 1 to highlight the TBG areas (green areas). In both parts a and b of Figure 4, the TBG is surrounded by a red dotted line for better visualization. The yellow regions cover single-layer graphene, and the blue regions on top indicate multilayer graphene. Figure 4c presents a representative micro-Raman spectrum of the same TBG. The spectrum was obtained with an excitation laser line of 532 nm. The first-order bond-stretching G mode, at 1582 cm^{-1},[40,41] exhibits a well-defined Lorentzian shape. The two-phonon 2D peak at 2686 cm^{-1} is associated with a totally symmetric transversal optical mode near the K point in the first Brillouin zone of graphene[40,41] and exhibits the broad shape typically observed in the Raman spectra of TBG samples with small θ ($\theta \leqslant 10°$).[29,42−44] There is no sign of any detectable defect-induced D band (expected at ≈1340 cm^{-1}) or any other peak related to contamination by organic compounds. The inset shows an image extracted from a hyperspectral Raman map, in which the color scale renders the 2D/G intensity ratio. The green shades (delineated by red dashed lines) span over the TBG area, the yellow shades cover single-layer graphene areas, and the blue shades indicate multilayer graphene.

The undetectable levels of the disorder-induced D band's intensity over the TBG samples produced by the tear-and-stack method indicate a low concentration of structural defects such as vacancies and grain boundaries.[45] However, besides structural defects, strain and doping also affect the operation of graphene-based devices, and Raman spectroscopy is able to detect and evaluate the levels of both of them as well.[46,47] Because both strain and doping influence the 2D and G bands' frequencies, the comparison between these two quantities provides a route to disentangle their Raman signatures. This schema was introduced by Lee et al.,[46] who proposed the plot of the 2D band's frequency (ω_{2D}) as a function of the G band's frequency (ω_G) to simultaneously analyze strain and doping in graphene by Raman spectroscopy. Although ω_{2D} varies linearly with ω_G for both strain and doping, the slopes are different, being 2.2 for hydrostatic strain (isodoping), 0.75 for p doping (isostrain), and ≈0.1 for n doping (isostrain). Intermediate values (between 0.75 and 2.2) can occur in systems where strain and doping coexist, and the crossing point indicates the absence of both.[46−48] Figure 4d shows the ω_{2D} versus ω_G plot of the data extracted from the hyperspectral Raman matrix that gave rise to the image shown in Figure 4b. Blue and red bullets are data points extracted from the areas delimited by the dashed blue and red lines, respectively. The lines with slopes of 2.2 (dashed black line) and 0.75 (dashed green line) are also plotted in Figure 4d for reference. The crossing point between the isostrain and isodoping lines in TBG may depend on twist-angle, laser-energy excitation, and its determination is beyond the scope of this work. All reference lines plotted in Figures 4 and 5 are guidelines, and their crossings have no real meaning. TBG samples on SiO_2 substrates are known to present spatially heterogeneous charge distributions.[49,50] As such, the blue bullets in Figure 4d, extracted from the TBG area, are widely spread over the plot, indicating the coexistence of strain and

https://dx.doi.org/10.1021/acsanm.0c03230
ACS Appl. Nano Mater. 2021, 4, 1858−1866

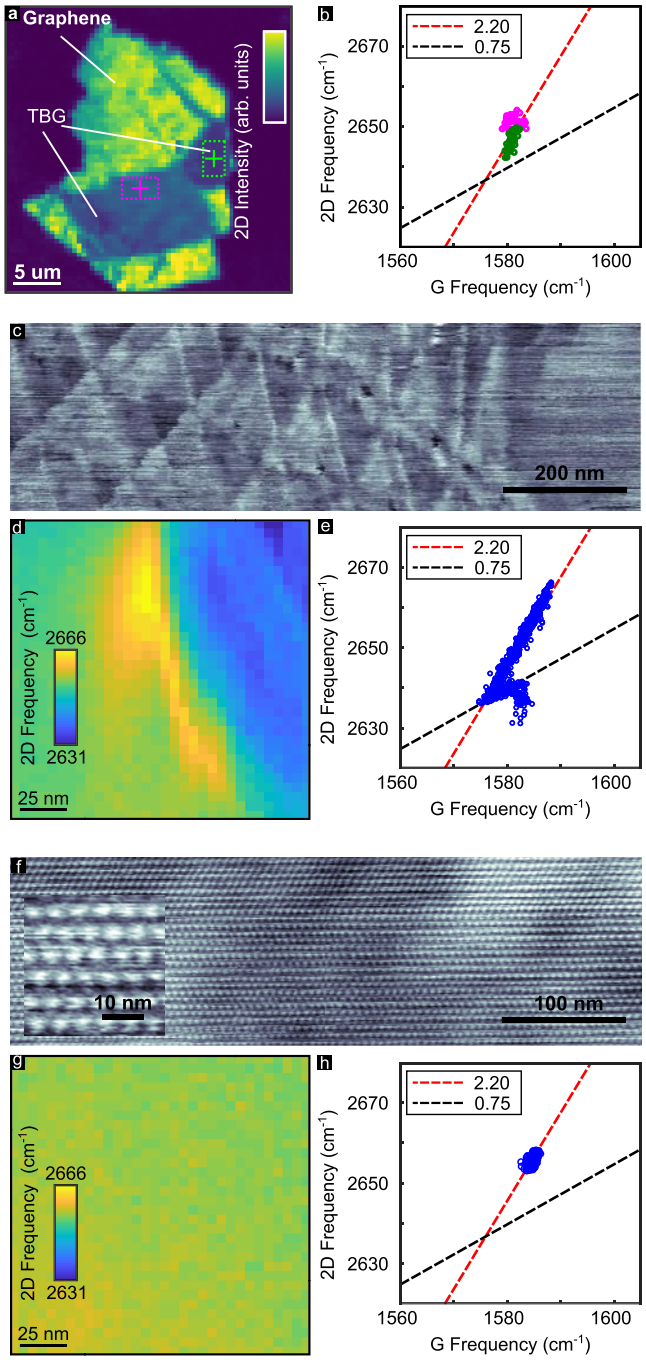

Figure 5. Micro- and nano-Raman analysis of the local strain in the TBG on a hBN substrate. (a) Micro-Raman hyperspectral map of a TBG sample sitting on a hBN substrate. The TBG + hBN system is deposited on a glass coverslip. The color scale renders the 2D band's intensity. (b) ω_{2D} versus ω_G plot extracted from the same micro-Raman hyperspectral matrix that gave rise to the image in panel a. The pink and green bullets were extracted from the dashed pink and green rectangular regions depicted in part a, respectively. (c) sMIM data showing the conductance component of the reflected microwave signal over the area highlighted by the red cross in panel a. (d) Nano-Raman hyperspectral map scanned over a 120 × 120 nm^2 area centered at the location indicated by the pink cross in panel a. The color scale renders the 2D band's frequency with a spacial resolution of ≈10 nm. (e) ω_{2D} versus ω_G plot for data (blue bullets) extracted from the nano-Raman hyperspectral matrix that gave rise to the image in panel d. (f and h) Similar to parts c−e, respectively, but the analysis was performed over the area highlighted by the green cross in panel a.

doping over the scanned area. By shrinking of the analyzed area down to a 15 μm × 5 μm rectangle, boxed by a red dashed line in Figure 4b from which the red bullets in Figure 4d were extracted, a considerably smaller spreading of the data points is observed. These data points (red bullets) present a subtle tendency to follow the 2.2 slope line, indicating strain, but micro-Raman spectroscopy is not able to precisely detect the local strain expected in TBGs because it lacks the necessary level of spatial resolution.

Not just the charge inhomogeneity impacts Raman analysis on TBG. In fact, micro-Raman spectroscopy fails to deliver accurate local distributions of strain or doping because it lacks spatial resolution due to diffraction.[51] The measurement is performed in the far-field regime, for which spatial resolution is limited to a half-wavelength of the excitation field (approximately 300 nm for visible light).[52] The information is blurred by spacial inhomogeneities.[53] To overcome this limitation, nano-Raman hyperspectral imaging, through the tip-enhanced Raman spectroscopy (TERS) schema, was employed.[52,54−59] Illumination and detection occur in the near-field regime through a nanoplasmonic structure.[52,60,61]

Figure 5a shows a micro-Raman hyperspectral map of a TBG sample sitting on a hBN substrate. Here a hBN substrate is used to overcome the interference of charge inhomogeneity on nano-Raman spectroscopy measurements. The spectrum was obtained with an excitation laser line of 633 nm. The color scale renders the 2D band's intensity, whose spatial variations indicate nonuniformity of structural parameters or charge distributions over the sample's surface. TBG and graphene areas span over the blue and yellow shades, respectively. Figure 5b shows the ω_{2D} versus ω_G plot extracted from the same micro-Raman hyperspectral matrix that gave rise to the image in Figure 5a. The pink and green bullets were extracted from the boxed areas delimited by the dashed pink and green rectangular regions of 4.0 μm × 2.5 μm in Figure 5a, respectively. The observed trend indicates the absence of local surface charge and the presence of a very small strain in the pink data compared to the green regions. Note that micro-Raman spatial resolution limits a precise interpretation because the data are acquired in an area larger than the unit cell of most of the Moiré superlattice formed in TBG.[2] Surely, a careful analysis of the Moiré superlattice has to be confronted with local Raman spectroscopy for a well-grounded interpretation.

Figure 5c shows a sMIM map obtained in the position indicated by the pink cross in Figure 5a. The image clearly shows the presence of a superstructure typical of reconstructed TBG (rTBG),[29,38] however, with the size of the reconstructed areas varying, indicating a gradient in strain from one layer with respect to the other (see more details in the Supporting Information). Figure 5d shows a nano-Raman hyperspectral map (TERS) scanned over a 120 × 120 nm^2 area also centered at the location indicated by the red cross in Figure 5a. The color scale renders the 2D band's frequency with a spacial resolution of ≈10 nm. Figure 5e shows the ω_{2D} versus ω_G plot for data (blue bullets) extracted from the nano-Raman hyperspectral matrix that gave rise to the image in Figure 5d. Most of the data points lie along the strain (red dashed) line or along the hole-doping (black dashed) line. The data points indicating high levels of strain correspond to the yellowish region in Figure 5d, consistent with the sMIM picture shown in Figure 5c. Because of experimental limitations, we cannot guarantee that parts c and d of Figure 5 come from exactly the same location, but they certainly come from close locations,

https://dx.doi.org/10.1021/acsanm.0c03230
ACS Appl. Nano Mater. 2021, 4, 1858−1866

and a larger microscopy picture of the region next to the pink cross in Figure 5a confirms that this region is indeed highly inhomogeneous with different rTBG formation, typical of a region with considerable strain gradients (see the Supporting Information).

A similar analysis was performed in the location indicated by the green cross in Figure 5a, and the results are displayed in Figures 5f–h. The results show that this region is much more uniform that the previous one, as visually shown in the sMIM map (Figure 5f) and also in the 2D band's nano-Raman frequency map (Figure 5g); both images are flat and practically featureless. The data points in the ω_{2D} versus ω_G plot (Figure 5h) are concentrated around a specific point of the strain line. The comparison between these two regions shows that nano-Raman spectroscopy is more than useful; it is rather a necessary tool to characterize TBG samples at the nanoscale, being able to indicate uniform areas, proper for device fabrication, unidentified by micro-Raman spectroscopy.

CONCLUSION

In conclusion, we created a deterministic and controllable nanomanipulation platform able to do a versatile tear-and-stack procedure as well as other possible manipulations. The twisted structures produced by this method are clean, as confirmed by micro- and nano-Raman imaging, sMIM, and STM. The PS technique does not require capping TBH with an hBN flake, which allows the study of these systems by many techniques. Our characterization based on Raman spectroscopy on TBG samples prepared on SiO_2 and hBN crystals shows that optical analysis can reveal whether the TBG region is under strain of doped-on hBN crystals, with nano-Raman showing details not observable in micro-Raman spectroscopy. We believe this work will provide new tools to the emerging field of twistronics, easing high-quality sample fabrication and characterization.

METHODS

Sample Preparation. We prepared the TBG samples by a new dry tear-and-stack method, using a PDMS semipyramidal stamp covered with a PC sheet. The method is similar to the standard tear-and-stack,[22,24] but here we use the PDMS stamp itself to tear a graphene flake into two pieces and stack them together, forming the TBG arrangement. Next, we transfer the TBG from the stamp to any substrate by detaching the PC at T = 180 °C. To prepare the rTBG from Figure 2a, we dry-transfer the TBG to a flat hBN flake. We do not heat the PC in this process; we make physical contact between the TBG and hBN flakes at room temperature. See the Supporting Information for more details.

sMIM. The sMIM data were acquired with a MFP-3D-SA atomic force microscope manufactured by Asylum Research. PrimeNano Inc. manufactured the specialized coaxial AFM probes and the microwave generator, mixer, and impedance matching circuitry. All sMIM data were collected at ambient conditions using a transmission signal of approximately 3 GHz.

STM. All STM data were collected with a UHV VT STM/AFM model manufactured by Omicron GmBH, which was previously calibrated against a standard graphite lattice of a HOPG surface well as against a reconstructed Si(111) 7 × 7 surface lattice. Etched W probes were used for all measurements performed at room temperature under a pressure of 1.0×10^{-10} Torr.

Micro-Raman and Nano-Raman Spectroscopy. Micro-Raman hyperspectral imaging was acquired on a Witec Alpha300 spectrometer. Nano-Raman hyperspectral imaging was acquired on a home-built system, through the TERS schema, and the technical details are explained in ref 62. Illumination and detection occur via a plasmon tunable tip pyramid,[63,64] whose apex diameter defines the spatial resolution (approximately 10 nm in the current case).

ASSOCIATED CONTENT

Supporting Information

The Supporting Information is available free of charge at https://pubs.acs.org/doi/10.1021/acsanm.0c03230.

Fabrication of the PS, transferring TBG from SiO_2 to mica/Au substrates, nano-Raman spectroscopy and TERS, and sMIM characterization of homogeneous and heterogeneous TBG on a hBN crystal (PDF)

AUTHOR INFORMATION

Corresponding Author

Leonardo C. Campos − *Physics Department, Universidade Federal de Minas Gerais, Belo Horizonte, Minas Gerais 31270-901, Brazil;* orcid.org/0000-0001-6792-7554; Email: lccampos@fisica.ufmg.br

Authors

Andreij C. Gadelha − *Physics Department, Universidade Federal de Minas Gerais, Belo Horizonte, Minas Gerais 31270-901, Brazil;* orcid.org/0000-0002-6350-7680

Douglas A. A. Ohlberg − *Microscopy Center, Universidade Federal de Minas Gerais, Belo Horizonte, Minas Gerais 31270-901, Brazil;* orcid.org/0000-0003-1634-0264

Fabiano C. Santana − *Physics Department, Universidade Federal de Minas Gerais, Belo Horizonte, Minas Gerais 31270-901, Brazil;* orcid.org/0000-0002-2169-5521

Gomes S. N. Eliel − *Instituto de Física, Universidade Federal da Bahia, Campus Universitário de Ondina, Salvador, Bahia 40170-115, Brazil; Instituto de Física, Universidade Federal Fluminense, Campus da Praia Vermelha, Niterói, Rio de Janeiro 24210-346, Brazil;* orcid.org/0000-0002-4658-3243

Jessica S. Lemos − *Physics Department, Universidade Federal de Minas Gerais, Belo Horizonte, Minas Gerais 31270-901, Brazil;* orcid.org/0000-0002-9493-9240

Vinícius Ornelas − *Physics Department, Universidade Federal de Minas Gerais, Belo Horizonte, Minas Gerais 31270-901, Brazil;* orcid.org/0000-0002-3636-7272

Daniel Miranda − *Physics Department, Universidade Federal de Minas Gerais, Belo Horizonte, Minas Gerais 31270-901, Brazil;* orcid.org/0000-0002-9784-3340

Rafael Battistella Nadas − *Physics Department, Universidade Federal de Minas Gerais, Belo Horizonte, Minas Gerais 31270-901, Brazil;* orcid.org/0000-0001-6165-5981

Kenji Watanabe − *National Institute for Materials Science, Tsukuba City, Ibaraki 305-0047, Japan;* orcid.org/0000-0003-3701-8119

Takashi Taniguchi − *National Institute for Materials Science, Tsukuba City, Ibaraki 305-0047, Japan;* orcid.org/0000-0002-1467-3105

Cassiano Rabelo − *Electrical Engineering and Technology Innovation Graduate Programs, Universidade Federal de Minas Gerais, Belo Horizonte, Minas Gerais 31270-901, Brazil;* orcid.org/0000-0003-0488-2242

Pedro Paulo de Mello Venezuela − *Instituto de Física, Universidade Federal Fluminense, Campus da Praia Vermelha, Niterói, Rio de Janeiro 24210-346, Brazil;* orcid.org/0000-0002-4166-2487

Gilberto Medeiros-Ribeiro − *Computer Science Department, Universidade Federal de Minas Gerais, Belo Horizonte,*

https://dx.doi.org/10.1021/acsanm.0c03230
ACS Appl. Nano Mater. 2021, 4, 1858−1866

Minas Gerais 31270-901, Brazil; orcid.org/0000-0001-5309-2488

Ado Jorio − *Physics Department, Universidade Federal de Minas Gerais, Belo Horizonte, Minas Gerais 31270-901, Brazil; Electrical Engineering and Technology Innovation Graduate Programs, Universidade Federal de Minas Gerais, Belo Horizonte, Minas Gerais 31270-901, Brazil;* orcid.org/0000-0002-5978-2735

Luiz Gustavo Cançado − *Physics Department, Universidade Federal de Minas Gerais, Belo Horizonte, Minas Gerais 31270-901, Brazil;* orcid.org/0000-0003-0816-0888

Complete contact information is available at: https://pubs.acs.org/10.1021/acsanm.0c03230

Notes

The authors declare no competing financial interest.

■ ACKNOWLEDGMENTS

This work was supported by CNPq, CAPES, INCT of Nanocarbono, and FAPEMIG. The authors are thankful to the UFMG Facilities: LCPNano and Centro de Microscopia. G.S.N.E. acknowledges FAPERJ for financial support. K.W. and T.T. acknowledge support from the Elemental Strategy Initiative conducted by the MEXT, Japan (Grant JPMXP0112101001), JSPS KAKENHI (Grant JP20H00354), and CREST, JST (Grant JPMJCR15F3). We are thankful to Dr. Alisson R. Cadore for discussions on sample preparation.

■ REFERENCES

(1) Cao, Y.; Fatemi, V.; Demir, A.; Fang, S.; Tomarken, S. L.; Luo, J. Y.; Sanchez-Yamagishi, J. D.; Watanabe, K.; Taniguchi, T.; Kaxiras, E.; Ashoori, R. C.; Jarillo-Herrero, P. Correlated insulator behaviour at half-filling in magic-angle graphene superlattices. *Nature* **2018**, *556* (7699), 80−84.

(2) Cao, Y.; Fatemi, V.; Fang, S.; Watanabe, K.; Taniguchi, T.; Kaxiras, E.; Jarillo-Herrero, P. Unconventional superconductivity in magic-angle graphene superlattices. *Nature* **2018**, *556* (7699), 43−50.

(3) Schmid, T.; Burkhard, J.; Yeo, B.; Zhang, W.; Zenobi, R. Towards chemical analysis of nanostructures in biofilms i: imaging of biological nanostructures. *Anal. Bioanal. Chem.* **2008**, *391* (5), 1899−1905.

(4) Sharpe, A. L.; Fox, E. J.; Barnard, A. W.; Finney, J.; Watanabe, K.; Taniguchi, T.; Kastner, M. A.; Goldhaber-Gordon, D. Emergent ferromagnetism near three-quarters filling in twisted bilayer graphene. *Science* **2019**, *365* (6453), 605−608.

(5) Wolf, T. M. R.; Lado, J. L.; Blatter, G.; Zilberberg, O. Electrically tunable flat bands and magnetism in twisted bilayer graphene. *Phys. Rev. Lett.* **2019**, *123*, 096802.

(6) Lu, X.; Stepanov, P.; Yang, W.; Xie, M.; Aamir, M. A.; Das, I.; Urgell, C.; Watanabe, K.; Taniguchi, T.; Zhang, G.; Bachtold, A.; MacDonald, A. H.; Efetov, D. K. Superconductors, orbital magnets and correlated states in magic-angle bilayer graphene. *Nature* **2019**, *574* (7780), 653−657.

(7) Yankowitz, M.; Chen, S.; Polshyn, H.; Zhang, Y.; Watanabe, K.; Taniguchi, T.; Graf, D.; Young, A. F.; Dean, C. R. Tuning superconductivity in twisted bilayer graphene. *Science* **2019**, *363* (6431), 1059−1064.

(8) Cao, Y.; Luo, J. Y.; Fatemi, V.; Fang, S.; Sanchez-Yamagishi, J. D.; Watanabe, K.; Taniguchi, T.; Kaxiras, E.; Jarillo-Herrero, P. Superlattice-induced insulating states and valley-protected orbits in twisted bilayer graphene. *Phys. Rev. Lett.* **2016**, *117* (11), 116804.

(9) Saito, Y.; Ge, J.; Watanabe, K.; Taniguchi, T.; Young, A. F. Independent superconductors and correlated insulators in twisted bilayer graphene. *Nat. Phys.* **2020**, *16*, 926−930.

(10) Balents, L.; Dean, C. R.; Efetov, D. K.; Young, A. F. Superconductivity and strong correlations in moiré flat bands. *Nat. Phys.* **2020**, *16*, 725−733.

(11) Carr, S.; Massatt, D.; Fang, S.; Cazeaux, P.; Luskin, M.; Kaxiras, E. Twistronics: Manipulating the electronic properties of two-dimensional layered structures through their twist angle. *Phys. Rev. B: Condens. Matter Mater. Phys.* **2017**, *95* (7), 075420.

(12) Isobe, H.; Yuan, N. F. Q.; Fu, L. Unconventional superconductivity and density waves in twisted bilayer graphene. *Phys. Rev. X* **2018**, *8* (4), 041041.

(13) Wu, F.; MacDonald, A. H.; Martin, I. Theory of phonon-mediated superconductivity in twisted bilayer graphene. *Phys. Rev. Lett.* **2018**, *121* (25), 257001.

(14) Wu, F.; Hwang, E.; Das Sarma, S. Phonon-induced giant linear-in-t resistivity in magic angle twisted bilayer graphene: Ordinary strangeness and exotic superconductivity. *Phys. Rev. B: Condens. Matter Mater. Phys.* **2019**, *99* (16), 165112.

(15) Culchac, F. J.; Del Grande, R. R.; Capaz, R. B.; Chico, L.; Morell, E. S. Flat bands and gaps in twisted double bilayer graphene. *Nanoscale* **2020**, *12* (8), 5014−5020.

(16) Shen, C.; Chu, Y.; Wu, Q.; Li, N.; Wang, S.; Zhao, Y.; Tang, J.; Liu, J.; Tian, J.; Watanabe, K.; Taniguchi, T.; Yang, R.; Meng, Z. Y.; Shi, D.; Yazyev, O. V.; Zhang, G. Correlated states in twisted double bilayer graphene. *Nat. Phys.* **2020**, *16* (5), 520−525.

(17) An, L.; Cai, X.; Huang, M.; Wu, Z.; Lin, J.; Ying, Z.; Ye, Z.; Feng, X.; Wang, N. Interaction effects and superconductivity signatures in twisted double-bilayer WSe_2. *arXiv:1907.03966*, 2019.

(18) Wang, L.; Shih, E.; Ghiotto, A.; Xian, L.; Rhodes, D. A.; Tan, C.; Claassen, M.; Kennes, D. M.; Bai, Y.; Kim, B.; Watanabe, K.; Taniguchi, T.; Zhu, X.; Hone, J.; Rubio, A.; Pasupathy, A. N.; Dean, C. R. Correlated electronic phases in twisted bilayer transition metal dichalcogenides. *Nat. Mater.* **2020**, *19*, 861−866.

(19) Suk, J. W.; Kitt, A.; Magnuson, C. W.; Hao, Y.; Ahmed, S.; An, J.; Swan, A. K.; Goldberg, B. B.; Ruoff, R. S. Transfer of cvd-grown monolayer graphene onto arbitrary substrates. *ACS Nano* **2011**, *5* (9), 6916−6924.

(20) Yang, S.; Choi, S.; Odongo Ngome, F. O.; Kim, K.; Choi, S.; Kim, C. All-dry transfer of graphene film by van der waals interactions. *Nano Lett.* **2019**, *19* (6), 3590−3596.

(21) Kinoshita, K.; Moriya, R.; Onodera, M.; Wakafuji, Y.; Masubuchi, S.; Watanabe, K.; Taniguchi, T.; Machida, T. Dry release transfer of graphene and few-layer h-bn by utilizing thermoplasticity of polypropylene carbonate. *npj 2D Materials and Applications* **2019**, *3* (1), 22.

(22) Pizzocchero, F.; Gammelgaard, L.; Jessen, B. S.; Caridad, J. M.; Wang, L.; Hone, J.; Boggild, P.; Booth, T. J. The hot pick-up technique for batch assembly of van der waals heterostructures. *Nat. Commun.* **2016**, *7* (1), 11894.

(23) Frisenda, R.; Navarro-Moratalla, E.; Gant, P.; Pérez De Lara, D.; Jarillo-Herrero, P.; Gorbachev, R. V.; Castellanos-Gomez, A. Recent progress in the assembly of nanodevices and van der waals heterostructures by deterministic placement of 2d materials. *Chem. Soc. Rev.* **2018**, *47* (1), 53−68.

(24) Kim, K.; Yankowitz, M.; Fallahazad, B.; Kang, S.; Movva, H. C. P.; Huang, S.; Larentis, S.; Corbet, C. M.; Taniguchi, T.; Watanabe, K.; Banerjee, S. K.; LeRoy, B. J.; Tutuc, E. van der waals heterostructures with high accuracy rotational alignment. *Nano Lett.* **2016**, *16* (3), 1989−1995.

(25) Jiang, Y.; Lai, X.; Watanabe, K.; Taniguchi, T.; Haule, K.; Mao, J.; Andrei, E. Y. Charge order and broken rotational symmetry in magic-angle twisted bilayer graphene. *Nature* **2019**, *573*, 91−95.

(26) Wakafuji, Y.; Moriya, R.; Masubuchi, S.; Watanabe, K.; Taniguchi, T.; Machida, T. 3d manipulation of 2d materials using microdome polymer. *Nano Lett.* **2020**, *20* (4), 2486−2492.

(27) Serlin, M.; Tschirhart, C. L.; Polshyn, H.; Zhang, Y.; Zhu, J.; Watanabe, K.; Taniguchi, T.; Balents, L.; Young, A. F. Intrinsic quantized anomalous hall effect in a moiré heterostructure. *Science* **2020**, *367* (6480), 900−903.

(28) Polshyn, H.; Yankowitz, M.; Chen, S.; Zhang, Y.; Watanabe, K.; Taniguchi, T.; Dean, C. R.; Young, A. F. Large linear-in-temperature resistivity in twisted bilayer graphene. *Nat. Phys.* **2019**, *15* (10), 1011−1016.
(29) Gadelha, A. C.; Ohlberg, D. A. A.; Rabelo, C.; Eliel, G. S. N.; Vasconcelos, T. L.; Campos, J. L.; Lemos, J. S.; Ornelas, V.; Miranda, D.; Nadas, R.; Santana, F. C.; Watanabe, K.; Taniguchi, T.; Troeye, B. V.; Lamparski, M.; Meunier, V.; Nguyen, V.; Paszko, D.; Charlier, J.; Campos, L. C.; Cançado, L. G.; Medeiros-Ribeiro, G.; Jorio, A. Lattice dynamics localization in low-angle twisted bilayer graphene. *arXiv:2006.09482*, 2020.
(30) Sunku, S. S.; Ni, G. X.; Jiang, B. Y.; Yoo, H.; Sternbach, A.; McLeod, A. S.; Stauber, T.; Xiong, L.; Taniguchi, T.; Watanabe, K.; Kim, P.; Fogler, M. M.; Basov, D. N. Photonic crystals for nano-light in moiré graphene superlattices. *Science* **2018**, *362* (6419), 1153−1156.
(31) Barboza, A. P. M.; Souza, A. C. R.; Matos, M. J. S.; Brant, J. C.; Barbosa, T. C.; Chacham, H.; Mazzoni, M. S. C.; Neves, B. R. A. Graphene/h-bn heterostructures under pressure: From van der waals to covalent. *Carbon* **2019**, *155*, 108−113.
(32) Utama, M. I. B.; Koch, R. J.; Lee, K.; Leconte, N.; Li, H.; Zhao, S.; Jiang, L.; Zhu, J.; Watanabe, K.; Taniguchi, T.; Ashby, P. D.; Weber-Bargioni, A.; Zettl, A.; Jozwiak, C.; Jung, J.; Rotenberg, E.; Bostwick, A.; Wang, F. Visualization of the flat electronic band in twisted bilayer graphene near the magic angle twist. *Nat. Phys.* **2020**, 1−5.
(33) Hou, Y.; Ren, X.; Fan, J.; Wang, G.; Dai, Z.; Jin, C.; Wang, W.; Zhu, Y.; Zhang, S.; Liu, L.; Zhang, Z. Preparation of Twisted Bilayer Graphene via the Wetting Transfer Method. *ACS Appl. Mater. Interfaces* **2020**, *12*, 40958−40967.
(34) Bistritzer, R.; MacDonald, A. H. Moiré butterflies in twisted bilayer graphene. *Phys. Rev. B: Condens. Matter Mater. Phys.* **2011**, *84* (3), 035440.
(35) Hunt, B.; Sanchez-Yamagishi, J. D.; Young, A. F.; Yankowitz, M.; LeRoy, B. J.; Watanabe, K.; Taniguchi, T.; Moon, P.; Koshino, M.; Jarillo-Herrero, P.; Ashoori, R. C. Massive dirac fermions and hofstadter butterfly in a van der waals heterostructure. *Science* **2013**, *340* (6139), 1427−1430.
(36) Dean, C. R.; Wang, L.; Maher, P.; Forsythe, C.; Ghahari, F.; Gao, Y.; Katoch, J.; Ishigami, M.; Moon, P.; Koshino, M.; Taniguchi, T.; Watanabe, K.; Shepard, K. L.; Hone, J.; Kim, P. Hofstadteras butterfly and the fractal quantum hall effect in moire superlattices. *Nature* **2013**, *497* (7451), 598−602.
(37) Moon, P.; Koshino, M. Electronic properties of graphene/hexagonal-boron-nitride moiré superlattice. *Phys. Rev. B: Condens. Matter Mater. Phys.* **2014**, *90* (15), 155406.
(38) Yoo, H.; Engelke, R.; Carr, S.; Fang, S.; Zhang, K.; Cazeaux, P.; Sung, S. H.; Hovden, R.; Tsen, A. W.; Taniguchi, T.; Watanabe, K.; Yi, G.; Kim, M.; Luskin, M.; Tadmor, E. B.; Kaxiras, E.; Kim, P. Atomic and electronic reconstruction at the van der waals interface in twisted bilayer graphene. *Nat. Mater.* **2019**, *18* (5), 448−453.
(39) Ohlberg, D.; Tami, D.; Gadelha, A.; Eliel, G. S. N.; Santana, F. C.; Miranda, D.; Avelino, W.; Watanabe, K.; Taniguchi, T.; Campos, L. C.; Ramirez, J. C.; Rego, C. G.; Jorio, A.; Medeiros-Ribeiro, G. The limits of near field immersion microwave microscopy evaluated by imaging bilayer graphene moiré patterns. *arXiv:2007.03823*, 2020.
(40) Malard, L. M.; Pimenta, M. A.; Dresselhaus, G.; Dresselhaus, M. S. Raman spectroscopy in graphene. *Phys. Rep.* **2009**, *473* (5), 51−87.
(41) Jorio, A.; Saito, R.; Dresselhaus, G.; Dresselhaus, M. S. *Raman Spectroscopy in Graphene Related Systems*; Wiley-VCH Verlag GmbH & Co. KGaA: Weinheim, Germany, 2011.
(42) Jorio, A.; Cançado, L. G. Raman spectroscopy of twisted bilayer graphene. *Solid State Commun.* **2013**, *175*, 3−12.
(43) Kim, K.; Coh, S.; Tan, L. Z.; Regan, W.; Yuk, J. M.; Chatterjee, E.; Crommie, M. F.; Cohen, M. L.; Louie, S. G.; Zettl, A. Raman spectroscopy study of rotated double-layer graphene: Misorientation-angle dependence of electronic structure. *Phys. Rev. Lett.* **2012**, *108*, 246103.
(44) Eliel, G. S. N.; Moutinho, M. V. O.; Gadelha, A. C.; Righi, A.; Campos, L. C.; Ribeiro, H. B.; Chiu, P.; Watanabe, K.; Taniguchi, T.; Puech, P.; Paillet, M.; Michel, T.; Venezuela, P.; Pimenta, M. A. Intralayer and interlayer electron-phonon interactions in twisted graphene heterostructures. *Nat. Commun.* **2018**, *9* (1), 1221.
(45) Gustavo Cançado, L. G.; Gomes da Silva, M.; Martins Ferreira, E. H.; Hof, F.; Kampioti, K.; Huang, K.; Pénicaud, A.; Alberto Achete, C.; Capaz, R. B.; Jorio, A. Disentangling contributions of point and line defects in the Raman spectra of graphene-related materials. *2D Mater.* **2017**, *4* (2), 025039.
(46) Lee, J. E.; Ahn, G.; Shim, J.; Lee, Y. S.; Ryu, S. Optical separation of mechanical strain from charge doping in graphene. *Nat. Commun.* **2012**, *3* (1), 1024.
(47) Mueller, N. S.; Heeg, S.; Alvarez, M. P.; Kusch, P.; Wasserroth, S.; Clark, N.; Schedin, F.; Parthenios, J.; Papagelis, K.; Galiotis, C.; Kalbáč, M.; Vijayaraghavan, A.; Huebner, U.; Gorbachev, R.; Frank, O.; Reich, S. Evaluating arbitrary strain configurations and doping in graphene with raman spectroscopy. *2D Mater.* **2018**, *5* (1), 015016.
(48) Ahn, G.; Ryu, S. Reversible sulfuric acid doping of graphene probed by in-situ multiwavelength Raman spectroscopy. *Carbon* **2018**, *138*, 257−263.
(49) Xue, J.; Sanchez-Yamagishi, J. D.; Bulmash, D.; Jacquod, P.; Deshpande, A.; Watanabe, K.; Taniguchi, T.; Jarillo-Herrero, P.; LeRoy, B. J. Scanning tunnelling microscopy and spectroscopy of ultra-flat graphene on hexagonal boron nitride. *Nat. Mater.* **2011**, *10* (4), 282−285.
(50) Zhang, Y.; Brar, V. W.; Girit, C.; Zettl, A.; Crommie, M. F. Origin of spatial charge inhomogeneity in graphene. *Nat. Phys.* **2009**, *5* (10), 722−726.
(51) Jorio, A.; Cançado, L. G.; Heeg, S.; Novotny, L.; Hartschuh, A. Tip-enhanced spectroscopy and imaging of carbon nanomaterials. *Handbook of Carbon Nanomaterials* **2019**, *10*, 175.
(52) Novotny, L.; Hecht, B. *Principles of Nano-Optics*; Cambridge University Press, 2012.
(53) Uri, A.; Grover, S.; Cao, Y.; Crosse, J. A.; Bagani, K.; Rodan-Legrain, D.; Myasoedov, Y.; Watanabe, K.; Taniguchi, T.; Moon, P.; Koshino, M.; Jarillo-Herrero, P.; Zeldov, E. Mapping the twist-angle disorder and landau levels in magic-angle graphene. *Nature* **2020**, *581* (7806), 47−52.
(54) Cançado, L. G.; Hartschuh, A.; Novotny, L. Tip-enhanced Raman spectroscopy of carbon nanotubes. *J. Raman Spectrosc.* **2009**, *40* (10), 1420−1426.
(55) Stadler, J.; Schmid, T.; Zenobi, R. Nanoscale Developments in and practical guidelines for tip-enhanced Raman spectroscopy. *Nanoscale* **2012**, *4*, 1856−1870.
(56) Mauser, N.; Hartschuh, A. Tip-enhanced near-field optical microscopy. *Chem. Soc. Rev.* **2014**, *43* (4), 1248−1262.
(57) Deckert-gaudig, T.; Taguchi, A.; Kawata, S.; Deckert, V. Tip-enhanced Raman spectroscopy-from early developments to recent advances. *Chem. Soc. Rev.* **2017**, *46*, 4077−4110.
(58) Shao, F.; Zenobi, R. Tip-enhanced raman spectroscopy: principles, practice, and applications to nanospectroscopic imaging of 2d materials. *Anal. Bioanal. Chem.* **2019**, *411* (1), 37−61.
(59) Rabelo, C.; Miranda, H.; Vasconcelos, T. L.; Cançado, L. G.; Jorio, A. Tip-enhanced Raman Spectroscopy of Graphene. *In 2019 4th International Symposium on Instrumentation Systems, Circuits and Transducers (INSCIT) - IEEE* **2019**, 1−6.
(60) Shi, X.; Coca-López, N.; Janik, J.; Hartschuh, A. Advances in Tip-Enhanced Near-Field Raman Microscopy Using Nanoantennas. *Chem. Rev.* **2017**, *117* (4), 4945−4960.
(61) Vasconcelos, T. L.; Archanjo, B. S.; Oliveira, B. S.; Silva, W. F.; Alencar, R. S.; Rabelo, C.; Achete, C. A.; Jorio, A.; Cançado, L. G. Optical nanoantennas for tip-enhanced raman spectroscopy. *IEEE J. Sel. Top. Quantum Electron.* **2021**, *27* (1), 1−11.
(62) Rabelo, C.; Miranda, H.; Vasconcelos, T. L.; Cançado, L. G.; Jorio, A. Tip-enhanced raman spectroscopy of graphene. *In 2019 4th International Symposium on Instrumentation Systems, Circuits and Transducers (INSCIT)* **2019**, 1−6.

https://dx.doi.org/10.1021/acsanm.0c03230
ACS Appl. Nano Mater. 2021, 4, 1858−1866

(63) Vasconcelos, T. L.; Archanjo, B.; Oliveira, B. S.; Valaski, R.; Cordeiro, R. C.; Medeiros, H. G.; Rabelo, C.; Ribeiro, A.; Ercius, P.; Achete, C. A.; Jorio, A.; Cançado, L. G. Plasmon-Tunable Tip Pyramids: Monopole Nanoantennas for Near-Field Scanning Optical Microscopy. Advanced. *Adv. Opt. Mater.* **2018**, *6* (20), 1800528.

(64) Miranda, H.; Rabelo, C.; Vasconcelos, T. L.; Cançado, L. G.; Jorio, A. Optical properties of plasmon-tunable tip pyramids for tip-enhanced raman spectroscopy. *Phys. Status Solidi RRL* **2020**, *14* (9), 2000212.

https://dx.doi.org/10.1021/acsanm.0c03230
ACS Appl. Nano Mater. 2021, 4, 1858−1866